Microgravity Science and Technology (2024) 36:15
https://doi.org/10.1007/s12217-024-10102-2

RESEARCH

Tracking the Motion of an Intruder Particle in a Three-Dimensional Granular Bed On-board the Chinese Space Station

Ke Cheng[1] · Meiying Hou[1] · Tuo Li[1] · Zhihong Qiao[2] · Peng Liu[2] · Jianzhi Ding[2] · Wei Sun[2] · Yuman Li[2] · Fade Gao[2] · Xiang Li[2] · Mingcheng Yang[1,3,4]

Received: 5 December 2023 / Accepted: 18 February 2024

Abstract
Three-dimensional (3D) particle tracking is a challenging task in dense granular systems. Magnetic particle tracking has been developed in recent years to reconstruct a tracer's trajectory in granular systems. The method can be low-cost, compact, and flexible. In this work we applied a Hall sensor array method to track the trajectories of a magnetic intruder particle in a 3D granular bed in the centrifuge of the Chinese Space Station (CSS). We present a developed algorithm. By placing sensors in an array in a same plane, our algorithm can exclude the interference of varying external field. The method's static accuracy can reach 0.02 cm, and the maximum deviation of our measurement from a known path is also checked to be 0.02 cm. On CSS, two independent sensor arrays are used to cross-check the accuracy of the method. The two measured trajectories are well overlapped. This confirms the method's reliability and robustness of tracking an intruder in a dense granular bed.

Keywords Granular matter · Particle tracking · Chinese Space Station · Hall sensors

Introduction

Tracking particles in three-dimensional (3D) systems is a challenging task that demands specialized equipment, algorithms, and techniques to achieve precise and dependable measurements. The complexity arises from the inherent variability and noise in the data, as well as the necessity to accurately trace small and swiftly moving particles. Unlike two-dimensional (2D) tracking, 3D particle tracking presents additional complexities, such as the need to handle occlusions, where particles may be obscured by other objects, making traditional image analysis techniques less effective.

Current 3D tracking methods in granular systems include, for example, Digital Image Correlation (DIC) (Hall et al. 2010), Particle Image Velocimetry (PIV) (Bokkers et al. 2004; Link et al. 2004; Liu et al. 2008), X-ray Computed Tomography (CT) (Andò et al. 2012; Schröter et al. 2022), electrical capacitance tomography (ECT) (Niedostatkiewicz et al. 2009; Mosorov et al. 2002; Wang et al. 2008), Magnetic Resonance Imaging (MRI) (Müller et al. 2006, 2007, 2008a, b; Ren et al. 2005), positron emission particle tracking (PEPT) (Link 2006; Wong 2006; Windows-Yule et al. 2020; Parker 2017; Marston and Thoroddsen 2015), radar tracking (Ott et al. 2017), ultrasonic tracking (van den Wildenberg et al. 2019), and fluorescence techniques (Karlsson et al. 2006). There are advantages and disadvantages of these methods. DIC is a non-contact method that uses image processing to track the displacement and deformation of a granular system. It is relatively fast and can provide a high spatial resolution, but it is limited in its ability to track particles that are transparent or have low contrast. PIV is similar to DIC, but it uses laser light to illuminate the particles and measure their velocity. It can provide high spatial and temporal resolution, but it is limited by the need for a seeding agent and the potential for image distortion caused by refraction. CT, ECT, and MRI are non-destructive methods, which use X-rays, electrical currents, and magnetic fields, respectively, to create detailed 3D images of a granular

✉ Meiying Hou
mayhou@iphy.ac.cn

[1] Beijing National Laboratory for Condensed Matter Physics and Laboratory of Soft Matter Physics, Institute of Physics, Beijing 100190, China

[2] Technology and Engineering Center for Space Utilization, Chinese Academy of Sciences, Beijing 100094, China

[3] School of Physical Sciences, University of Chinese Academy of Sciences, Beijing 100049, China

[4] Songshan Lake Materials Laboratory, Dongguan 523808, Guangdong, China

Published online: 07 March 2024

system. It can provide high spatial resolution, but it is limited by its high cost and the need for a radiation source, a conductive medium and/or a magnetic field, respectively. PEPT is a non-destructive method that uses radioactive particles to track the movement of individual particles in a granular system. It can provide high temporal resolution, but it is limited by its high cost and the need for a radioactive source. Ultrasonic tracking is also a non-destructive method, provides high temporal resolution, but is limited by its sensitivity to the properties of the particles and the surrounding medium. Fluorescence techniques use a fluorescent dye to track the movement of individual particles. They can provide high temporal resolution, but they are limited by the need for a fluorescent dye and the potential for the dye to interfere with the properties of the particles. A good overview on particle tracking in granular media can also be found in article by Schröter et al. (2022).

Mohs et al. developed in 2009 a magnetic particle monitoring method (Mohs et al. 2009) designed for use in a non-transparent granular spouted bed. Anisotropic magnetoresistive (AMR) sensors surrounding the granular bed detect the magnetic field of the tracer particle, and the particle's position is determined from the detected intensity of the magnetic field. While the spatial precision of this method has improved to 0.6% in recent years (Buist et al. 2014, 2015; Idakiev and Mörl 2013; Tao et al. 2019; Buist et al. 2017; Mema et al. 2020), it is limited to quasi-stationary external magnetic fields and requires the extensive placement of at least nine modules around the bed.

This paper presents a novel approach using Hall-effect magnetic sensor arrays to reconstruct the trajectories of a magnetic sphere within a vibro-fluidized three-dimensional granular bed housed in a centrifuge for reduced gravity aboard the CSS. The Hall effect, which induces a voltage perpendicular to both the current and the magnetic field when a current-carrying conductor is placed in a magnetic field, has been widely used for constructing transducers measuring magnetic fields in laboratory and research settings. The use of the Hall effect for tracking particles began to be explored in the early 2000s (Schlageter et al. 2001, 2002), especially in recent years being applied to medical instrumentation positioning applications (Vergne et al. 2023; Song et al. 2014; Hu et al. 2007). Our device, employing Hall sensors in an array, achieves compactness to meet the constraints of limited experimental volume, space, power, and flexibility in the Space Station. As the experimental chamber rotates with the centrifuge, the geomagnetic field direction changes periodically relative to the chamber. This paper introduces a new algorithm capable of precisely tracking particles under the evolving external geomagnetic field. The method's temporal fluctuations and spatial accuracy are demonstrated, showcasing a 3D trajectory reconstruction of an intruder immersed in the vibrated granular bed in reduced gravity within the CSS. With the current reliability and robustness, future developments aim to reduce the array size while increasing precision through adjustments in data sampling rates.

Experimental Setup and Algorithm

The experimental scheme is shown in Fig. 1(a). An intruder made of copper of diameter 1.0 cm with embedded permanent magnet (PM), is placed inside of a cubic container with 70 mm on each side. The container is filled to a height of 50 mm with spherical glass beads ranging in diameter from 0.6 mm to 0.8 mm. The intruder's movement within the granular bed is tracked using a Hall-sensor array placed at xOy plane of the container.

We establish the reference point for vertical position as $Z = 5$ cm when the intruder is at the surface, and $Z = 0.5$ cm when it is located at the bottom of the container. The intrusion coordinates (X, Y, Z) of the magnetic sphere are derived from the electric signals of the sensor array. The basic working principle of the Hall sensor is depicted in Fig. 1(b). The array consists of 7 sensors in a row and total 15 rows of sensors on a plate located in xOy plane. The plate is positioned at a distance exceeding 2.5 times the sphere's magnet size (about 0.6 cm in length), allowing us to treat the sphere as a magnetic dipole.

The magnetic induction intensity B of each sensor is a function of the position coordinates (X, Y, Z) and Euler angles (α, β) of the sphere. To determine the position coordinates (X, Y, Z) and the Euler angles (α, β) of the sphere, we employ the Levenberg-Marquardt fitting method (Levenberg 1944; Marquardt 1963) to invert the 105 over-determined equations of data collected by the array consisting of 105 Melexis MLX90393 3D magnetic sensors. The Levenberg-Marquardt algorithm is fast convergent and insensitive to the initial values of parameters. It is based on weighted least squares method, iteratively updating parameters by adjusting the step size in each iteration until the parameters converge to the optimal value, making it an effective method for curve fitting.

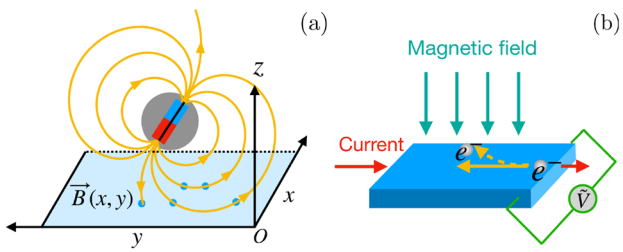

Fig. 1 **a** the experiment diagram. **b** the basic principle of Hall sensors. The array of 7×15 Hall sensors is located at xOy plane

These sensors, spaced 1 cm apart, boast a magnetic resolution 0.15 μT in the x and y axes, and 0.25 μT in the z axis. Additionally, they exhibit a sensitivity of 3.22 μT/LSB (LSB: least significant bit) in the x and y axes, and 5.87 μT/LSB in the z axis.

Operating at a sampling rate of 30 samples/sec, the sensor array dynamically captures the magnetic field measurements. This facilitates real-time tracking of the magnetic sphere's motion trajectory within the granular bed, as well as the acquisition of its rotation angle during its motion.

Each sensor located at coordinates (x, y) is capable of reading a magnetic field vector $\mathbf{B}$, where $\mathbf{B}(x, y)$ generally comprises four terms, as expressed by Eq. (1):

$$B_i^{(j)}(x,y) = C_i^{(j)} + G_i(x,y) + f_i^{(j)}(x,y) + \eta_i^{(j)} \tag{1}$$

Here, the index i corresponds to the Cartesian coordinates (x, y, z), and the index j represents the frame number. To ensure robustness of the results, we exclusively consider B_z for particle position determination. It is because all the sensors lie in the same plane and share a common z-axis. The contour of B_z contains only one peak and one valley, while for contours of B_x and B_y, each contains two peaks and two valleys. The fitting of B_x and B_y may cause unreasonable results. The reliability and robustness of utilizing B_z for particle positioning will be demonstrated later.

The first term $C_i^{(j)}$ represents the external magnetic field, such as the geomagnetic field. In our algorithm, since all sensors lie in the same plane and share a common z-axis, each sensor shares a same z component of the external magnetic field, and $C_z^{(j)}$ is invariant in space. The second term $G_z(x, y)$ represents the background magnetic field around the sensor array generated by the instruments near the sensor array. $G_z(x, y)$ remains constant with time. The third term $f_z^{(j)}(x, y)$ originates from the magnetic dipole in the sphere and is determined by the particle coordinates (X, Y, Z) and Euler angles (α, β) of the permanent magnet (PM). The fourth term $\eta_z^{(j)}$ arises from the noise of the ADC (analog-digital converter) of the array.

The background field $G_z^{(j)}(x, y)$ can be measured by removing the intruder and averaging the signal over M frames:

$$G_z(x,y) = \frac{1}{M}\sum_{j=1}^{M} G_z^{(j)}(x,y). \tag{2}$$

Usually the value of M can take a few thousand.

If the intruder remains relatively stationary over N frames, it is possible to mitigate fluctuations by applying data smoothing across those N frames. Under such quasi-static conditions, Eq. (1) undergoes a transformation as follows:

$$\begin{aligned} &f_z^{(j)}(x,y) + C_z^{(j)} + \frac{1}{N}\sum_{j}^{j+N-1} \eta_z^{(j)} \\ &= \frac{1}{N}\sum_{j}^{j+N-1} [B_z^{(j)}(x,y) - G_z(x,y)]. \end{aligned} \tag{3}$$

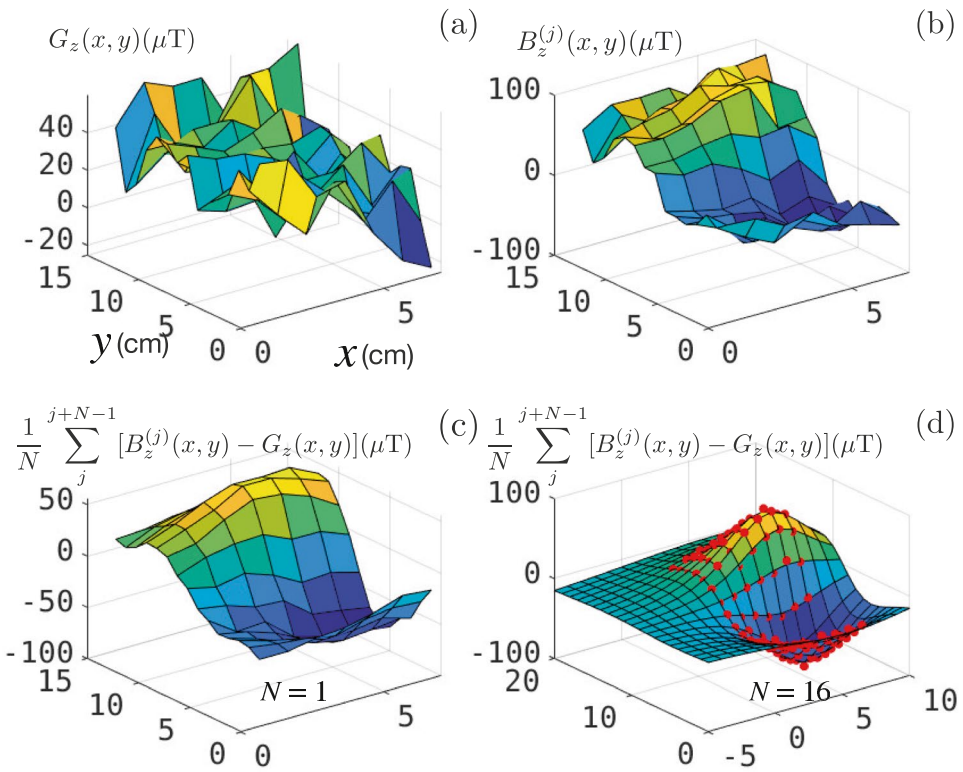

Fig. 2 **a** the background magnetic field $G_z(x, y)$. **b** the total magnetic field $B_z^{(j)}(x, y)$. **c** the result after subtracting the background $G_z(x, y)$ with the smoothing factor $N = 1$. **d** The red points for smoothing factor $N = 16$, and the surface is the fitting result with Eq. (7)

The right-hand side (rhs) of Eq. (3) can be experimentally measured. Figure 2(a) gives an example of background signal, and Fig. 2(b) is the measured total signal B_z. After subtracting the background $G_z(x, y)$, the result is illustrated in Fig. 2(c), comprising the dipole term $f_z^{(j)}(x, y)$, the geomagnetic field $C_z^{(j)}$, and the noise term $\eta_z^{(j)}$, as described in Eq. (3). Averaging the adjacent N frames, the noise can be significantly diminished, as shown in Fig. 2(d).

For the left-hand side (lhs) of Eq. (3), $f_z^{(j)}(x, y)$ can be readily obtained by considering the permanent magnet (PM) as a dipole. Assuming the half-length of the magnet is represented by d, the coordinates of the magnet poles are

$$\begin{aligned}\begin{pmatrix} x_1 \\ y_1 \\ z_1 \end{pmatrix} &= M_1 M_2 \begin{pmatrix} 0 \\ 0 \\ d \end{pmatrix} + \begin{pmatrix} X \\ Y \\ Z \end{pmatrix}, \\ \begin{pmatrix} x_2 \\ y_2 \\ z_2 \end{pmatrix} &= M_1 M_2 \begin{pmatrix} 0 \\ 0 \\ -d \end{pmatrix} + \begin{pmatrix} X \\ Y \\ Z \end{pmatrix},\end{aligned} \tag{4}$$

where $M_1$and M_2 are rotating matrices of α and β:

$$\begin{aligned} M_1 &= \begin{pmatrix} 1 & 0 & 0 \\ 0 & \cos(\alpha) & -\sin(\alpha) \\ 0 & \sin(\alpha) & \cos(\alpha) \end{pmatrix}, \\ M_2 &= \begin{pmatrix} \cos(\beta) & 0 & -\sin(\beta) \\ 0 & 1 & 0 \\ \sin(\beta) & 0 & \cos(\beta) \end{pmatrix}. \end{aligned} \tag{5}$$

The magnetic scalar potential in space can be written as:

$$\begin{aligned}\phi = &\frac{k}{\sqrt{(x-x_1)^2+(y-y_1)^2+(z-z_1)^2}} \\ &- \frac{k}{\sqrt{(x-x_2)^2+(y-y_2)^2+(z-z_2)^2}},\end{aligned} \tag{6}$$

where k is the strength of the magnet dipole. Therefore, the magnetic field in xOy plane can be written as $f_z^{(j)}(x, y) = \partial_z \phi|_{z=0}$. After some algebra,

$$\begin{aligned} f_z^{(j)}(x,y) + C_z^{(j)} = &k(d\cos\alpha\cos\beta - Z)\cdot[(d\cos\alpha\cos\beta - Z)^2 \\ &+ (-d\sin\beta - X + x)^2 \\ &+ (-d\sin\alpha\cos\beta - Y + y)^2]^{-3/2} \\ &+ k(d\cos\alpha\cos\beta + Z)\cdot[(d\cos\alpha\cos\beta + Z)^2 \\ &+ (d\sin\beta - X + x)^2 \\ &+ (d\sin\alpha\cos\beta - Y + y)^2]^{-3/2} + C_z^{(j)}. \end{aligned} \tag{7}$$

The measured half-length d of the PM is equal to 0.285 cm and the magnetic strength $k = 2.77 \times 10^4\ \mu\mathrm{T}\cdot\mathrm{cm}^2$. As (x, y) can take $7 \times 15 = 105$ discrete values, which is significantly greater than the number of unknowns, Eq. (7) forms a system of overdetermined equations. Consequently, it is more efficient to conduct fitting rather than seeking an analytical solution. From Eq. (7), by treating the coordinates (X, Y, Z), Euler angles (α, β) and the scalar $C_z^{(j)}$ as the fitting parameters, we are able to determine the particle location. Using MATLAB, we choose $X = Y = Z = 0, \alpha = 0, \beta = 0$ as initial fitting values. The damping parameter is chosen dynamically based on the curvature of the objective function. The method starts with a small initial value for the damping parameter and then evaluates the improvement in the objective function after each iteration. If the improvement is not significant, the damping parameter is increased to help converge to a better solution. If the improvement is too large, the damping parameter is decreased to prevent overshooting the optimal solution. As depicted in Fig. 2(d), the experimentally measured data points align well with Eq. (7). It shows the location of the particle can be accurately determined.

The signal-to-noise ratio of the magnetic field decreases as Z increases. In order to choose the worst case scenario, we placed the intruder at the surface of the granular bed, a position farthest away from the sensor array, to investigate the variation of the temporal fluctuations as a function of the smoothing factor N. The fluctuations of the particle position (X, Y, Z) are shown in Fig. 3(a)–(c). Indicated in Fig. 3(d), smoothing N adjacent frames reduces fluctuations by $1/\sqrt{N}$, as depicted by the red curve. With $N = 16$, the

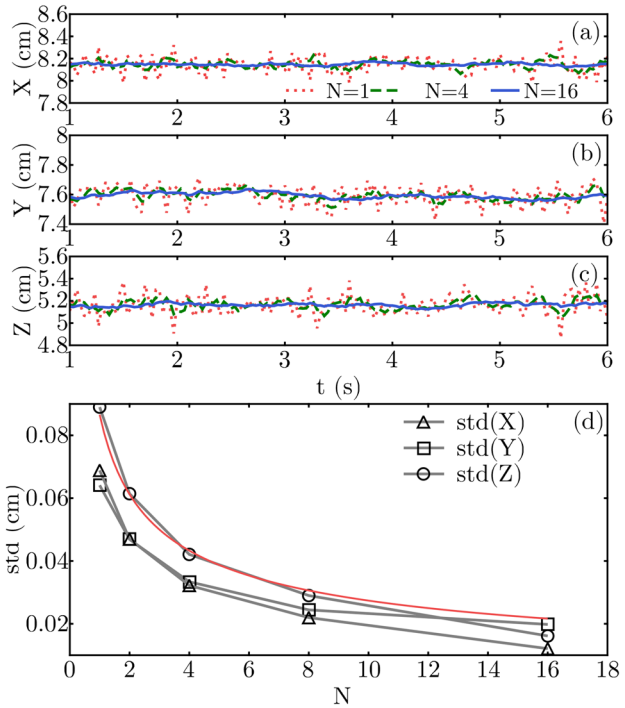

Fig. 3 **a**–**c** are the temporal fluctuations of the position (X, Y, Z) of the fixed particle. Red dots for $N = 1$, green dashed curve for $N = 4$ and blue solid curve for $N = 16$. **d** is the standard deviation for different N. Triangles, squares and circles represent for X, Y and Z respectively. The red curve is the fitted result for $\mathrm{std}(Z) \propto 1/\sqrt{N}$

standard deviation of Z is 0.02 cm. The smoothing procedure enhances measurement accuracy.

To assess spatial accuracy, we placed the sensor array vertically and secured a circular track on the horizontal plane. The diameter of the circular track is 6.8 cm, and we allowed the intruder to move along the track at a speed of 0.5 cm/s.

As illustrated in Fig. 4, the reconstructed trajectory represented by the blue points matches with the real trajectory of the intruder (depicted as red circles in Fig. 4). As the intruder moves farther away from the sensor array, the signal-to-noise ratio of the magnetic field diminishes, potentially resulting in increased errors in the measurement outcomes. However, this error can be mitigated by appropriately increasing the smoothing factor N. With $N \geq 16$, the standard deviation of the error remains below 0.02 cm ($Z = 6$ cm), even when the position is significantly distant from the sensor array.

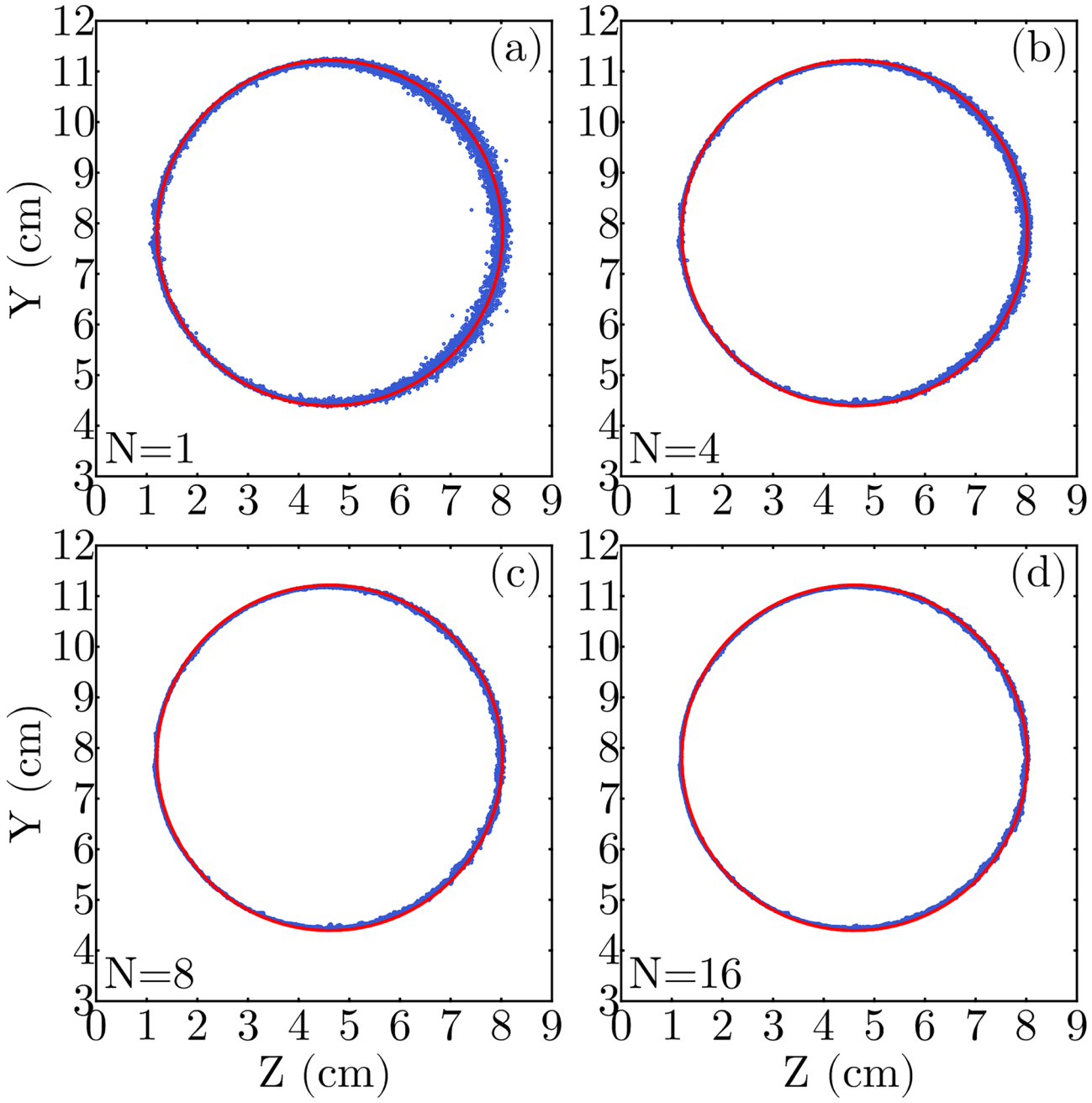

Fig. 4 The spatial accuracy for different smoothing factor N. Red circles are the exact track of the intruder, blue dots are the magnetic measurement result

Particle Tracking in Granular Bed on Board the CSS

The tracking method is applied for detection of the trajectory of a magnetic intruder in a vibration-driven granular chamber within a centrifuge of radius 90 cm. As depicted in Fig. 5(b), the artificial gravity acts in the opposite direction along the z-axis. The chamber, driven by a linear motor in the z-direction, has dimensions of 7 cm × 15 cm × 7 cm, equally divided into two compartments $B1$ and $B2$, both filled with glass beads. The magnetic sphere is positioned in compartment $B1$.

Firstly, we need to measure the gradient of the total magnetic field in order to estimate the influence of the total magnetic field on the intruder motion. We take out the intruder and let the linear motor move a distance of $2d = 5.7$ mm along the z axis. Then the variation of the magnetic field near the xOy plane is measured as ΔG_z. The magnetic force on the intruder is:

$$|F_z| \leq \frac{\Delta G_z}{\mu_0} q_m \tag{8}$$

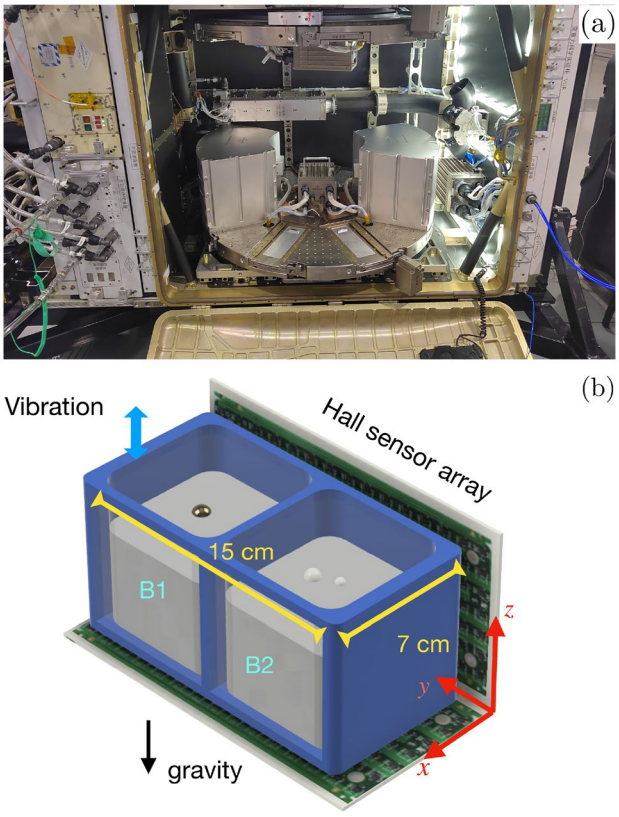

Fig. 5 **a** the chamber in the centrifuge on CSS. **b** the schematic diagram of the chamber. The vibration direction is along the z axis, and two sensor arrays are located on the xOy and yOz planes

This force takes its maximum value when the dipole is perpendicular to the xOy plane. The measured difference $\Delta G_z = 0.115\ \mu$T. μ_0 is the vacuum permeability, and the magnetic charge of the dipole is $q_m = 4\pi k$. At the bottom of the chamber, the force is $|F_z| = 3 \times 10^{-6}$ N. This is much smaller than the artificial gravitational force at 0.1g on the sphere (4.11×10^{-3} N). Therefore, we prove that the influence of the environmental magnetic field to the intruder can be neglected.

To cross-check the measurement accuracy, two Hall sensor arrays are placed at the xOy and yOz planes of the experimental chamber. The motion of the intruder is detected by both sensor arrays. Figure 6 shows the particle trajectory with vibration frequency $f = 5$ Hz and amplitude $A = 3.78$ mm under environmental gravity 0.1 g. The particle began to move at $t = 1250$ s when the chamber began to vibrate. It moves from the bottom to $z = 4$ cm and fluctuates at that height. The (X, Y, Z) components of the particle trajectory are shown in Fig. 6(a), and its corresponding 3D motion is shown in Fig. 6(d). The orientations of the dipole are shown in Fig. 6(b), where θ and ϕ are directions of the dipole projected on the xOy and yOz planes. The trajectories and orientations measured by the two sensor arrays nearly overlap. Due to the symmetry of the magnetic field, the rotation of the magnetic dipole around the axis of symmetry has no effect on the magnetic field, so the third Euler angle cannot be measured. If one is interested in this angle, it can be measured with a magnetic quadrupole.

The choice of the N value is determined by the signal to noise ratio. In Fig. 6(a), the intruder trajectory for $N = 1$ is given, and the inset gives the averaged trajectory for $N = 8$. Bed particles are agitated along Z direction. We expect the intruder particle moves mainly along Z direction, either ascent or descent. As seen in Fig. 6(a), the ascent velocities of the intruder are all measured as 0.39 cm/s both for $N = 1$ and $N = 8$. The spatial accuracy can be further improved by increasing the data sampling rate. Currently we are using a low rate 30 fps, which can easily be increased to 120 fps or even higher. In this case the spatial accuracy can be improved to 0.01 cm, much smaller than the instantaneous sharp turning distances observed in the Fig. 6(a).

The parameter $C_z^{(j)}$ represents the external magnetic field. In our experimental condition, it shall be the geomagnetic field in the chamber frame. We therefore examine the fitting results of $C_z^{(j)}$, plotted in Fig. 6(b). The red dashed curve represents the measurement of the xOy array, and the blue solid curve represents that of the yOz array. Both curves are cosine functions with a period $T = 3.9$ s, consistent with the rotation period of the centrifuge. The red and blue curves have amplitudes of 78.4 and 77.3, respectively. The phase of the red curve is $\pi/2$ ahead of the blue curve, attributed to

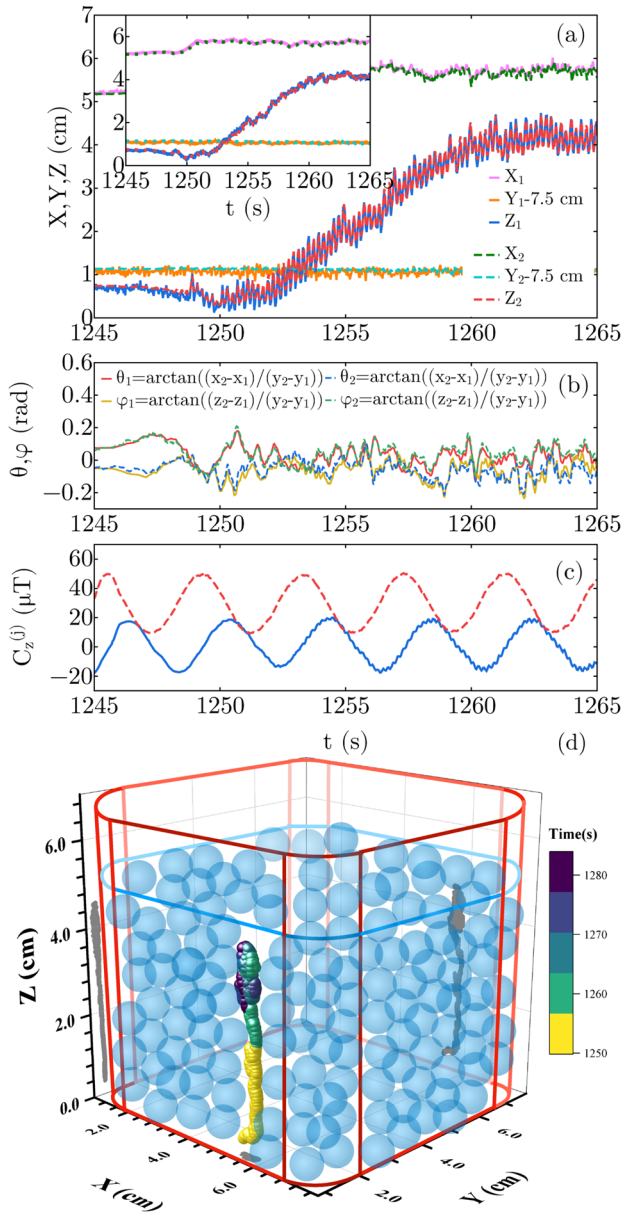

Fig. 6 **a** the three-dimensional position of the intruder for $N = 1$, the dots for xOy array, and solid curves for yOz array. The inset is for $N = 8$. **b** (θ_1, φ_1) and (θ_2, φ_2) are the directions of the dipole measured by the yOz and xOy array at $N = 8$. Dashed curves for (θ_1, φ_1), solid curves for (θ_2, φ_2). **c** the geomagnetic field $C_z^{(j)}$ of two arrays as functions of time, the red dashed curve for xOy array and the blue solid curve for yOz array. N is chosen as 8. **d** the three-dimensional trajectory of the intruder. The frame of solid red curves is the experimental chamber. The blue dashed outline indicates the surface of the granular bed

the geomagnetic field being projected into two mutually perpendicular planes, xOy and yOz. This verifies the fitting parameter $C_z^{(j)}$ is closely related to the external geomagnetic field, and our method is reliable.

Conclusions

In this work a new algorithm capable of precisely tracking particles under the evolving external geomagnetic field is presented. At the sampling rate of 30 fps, the spatial accuracy of the measurements of two perpendicularly placed Hall sensor arrays are cross-checked. The spatial accuracy measured by both arrays is 0.035 cm, showcasing a 3D trajectory reconstruction of an intruder immersed in a dense vibrated granular bed in reduced gravity within the CSS.

We prove that we can successfully track the motion of a single magnetic particle in a shaken granular bed. The algorithm proposed here is much simpler than the previous ones and is more time-efficient to implement. The signal to noise ratio can be improved by averaging the sampling rate by N frames. In our case we have chosen N to be 8 for most of the data. There are only 5 unknowns in Eq. (7). Current 105 sensors is much more than the number of unknowns for solving the equation. Thus a reasonable reduction in the number of sensors will not affect the fitting results. In addition, reducing the number of sensors can further increase the data sampling rate, and decrease the array size. With the current reliability and robustness, future developments aim to miniaturize the device while increasing precision through adjustments in data sampling rates.

The method is applicable to intruder tracking tasks in dense granular bed as long as geomagnetic influence is negligible compared to that of particle collisions or frictions. If rotational degrees of freedom are not of the concern, the method can also be applied to intruder tracking in granular gas.

Author Contributions Ke Cheng developed the algorithm and processed the experimental data. Meiying Hou wrote the draft and is responsible for the research. Tuo Li and Mingcheng Yang participate in the discussion. Zhihong QIao, Peng Liu, Jianzhi Ding, Wei Sun, Yuman Li, Fade Gao and Xiang Li are responsible for the instrumentation.

Funding This study is supported by the Space Application System of China Manned Space Program YYWT-0601-EXP-20, the ESA-CMSA/CSU Space Scince and Utilization collaboration program, and the National Key R&D Program of China (2022YFF0503504). K.C. and T.L. would like to thank the support by Wenzhou Institute, University of Chinese Academy of Sciences.

Data Availability The datasets generated during the current study are available from the corresponding author on reasonable request.

Declarations

Ethics Approval Not applicable.

Consent to Participate and Publish All the authors have agreed to participate and publish.

Competing Interests The authors declare no competing interests.

References

Andò, E., Hall, S.A., Viggiani, G., Desrues, J., Bésuelle, P.: Grain-scale experimental investigation of localised deformation in sand: a discrete particle tracking approach. Acta Geotech. **7**, 1–13 (2012)

Bokkers, G., Sint Annaland, M., Kuipers, J.: Mixing and segregation in a bidisperse gas-solid fluidised bed: a numerical and experimental study. Powder Technol. **140**(3), 176–186 (2004)

Buist, K.A., Gaag, A.C., Deen, N.G., Kuipers, J.A.: Improved magnetic particle tracking technique in dense gas fluidized beds. AIChE J. **60**(9), 3133–3142 (2014)

Buist, K., Van Erdewijk, T., Deen, N., Kuipers, J.: Determination and comparison of rotational velocity in a pseudo 2-d fluidized bed using magnetic particle tracking and discrete particle modeling. AIChE J. **61**(10), 3198–3207 (2015)

Buist, K.A., Jayaprakash, P., Kuipers, J., Deen, N.G., Padding, J.T.: Magnetic particle tracking for nonspherical particles in a cylindrical fluidized bed. AIChE J. **63**(12), 5335–5342 (2017)

Hall, S.A., Muir Wood, D., Ibraim, E., Viggiani, G.: Localised deformation patterning in 2D granular materials revealed by digital image correlation. Granul. Matter **12**, 1–14 (2010)

Hu, C., Meng, M.Q.-H., Mandal, M.: A linear algorithm for tracing magnet position and orientation by using three-axis magnetic sensors. IEEE Trans. Magn. **43**(12), 4096–4101 (2007)

Idakiev, V., Mörl, L.: How to measure the particle translation and rotation in a spouted and fluidized bed. J. Chem. Technol. Metall. **48**(5), 445–450 (2013)

Karlsson, S., Björn, I.N., Folestad, S., Rasmuson, A.: Measurement of the particle movement in the fountain region of a Wurster type bed. Powder Technol. **165**(1), 22–29 (2006)

Levenberg, K.: A method for the solution of certain non-linear problems in least squares. Q. Appl. Math. **2**(2), 164–168 (1944)

Link, J.M.: Development and validation of a discrete particle model of a spout-fluid bed granulator. Ph.D. Thesis, University of Twente, Netherlands (2006)

Link, J., Zeilstra, C., Deen, N., Kuipers, H.: Validation of a discrete particle model in a 2D spout-fluid bed using non-intrusive optical measuring techniques. Can. J. Chem. Eng. **82**(1), 30–36 (2004)

Liu, G.-Q., Li, S.-Q., Zhao, X.-L., Yao, Q.: Experimental studies of particle flow dynamics in a two-dimensional spouted bed. Chem. Eng. Sci. **63**(4), 1131–1141 (2008)

Marquardt, D.W.: An algorithm for least-squares estimation of nonlinear parameters. SIAM J. Appl. Math. **11**(2), 431–441 (1963)

Marston, J.O., Thoroddsen, S.T.: Investigation of granular impact using positron emission particle tracking. Powder Technol. **274**, 284–288 (2015)

Mema, I., Buist, K.A., Kuipers, J., Padding, J.T.: Fluidization of spherical versus elongated particles: Experimental investigation using magnetic particle tracking. AIChE J. **66**(4), 16895 (2020)

Mohs, G., Gryczka, O., Heinrich, S., Mörl, L.: Magnetic monitoring of a single particle in a prismatic spouted bed. Chem. Eng. Sci. **64**(23), 4811–4825 (2009)

Mosorov, V., Sankowski, D., Dyakowski, T., et al.: The 'best-correlated pixels' method for solid mass flow measurements using electrical capacitance tomography. Meas. Sci. Technol. **13**(12), 1810 (2002)

Müller, C.R., Holland, D.J., Sederman, A.J., Mantle, M.D., Gladden, L.F., Davidson, J.: Magnetic resonance imaging of fluidized beds. Powder Technol. **183**(1), 53–62 (2008a)

Müller, C., Davidson, J., Dennis, J., Fennell, P., Gladden, L., Hayhurst, A., Mantle, M., Rees, A., Sederman, A.: Oscillations in gas-fluidized beds: Ultra-fast magnetic resonance imaging and pressure sensor measurements. Powder Technol. **177**(2), 87–98 (2007)

Müller, C.R., Davidson, J.F., Dennis, J.S., Fennell, P., Gladden, L.F., Hayhurst, A.N., Mantle, M.D., Rees, A., Sederman, A.J.: Real-time measurement of bubbling phenomena in a three-dimensional gas-fluidized bed using ultrafast magnetic resonance imaging. Phys. Rev. Lett. **96**(15), 154504 (2006)

Müller, C.R., Holland, D.J., Sederman, A.J., Scott, S.A., Dennis, J.S., Gladden, L.F.: Granular temperature: comparison of magnetic resonance measurements with discrete element model simulations. Powder Technol. **184**(2), 241–253 (2008b)

Niedostatkiewicz, M., Tejchman, J., Chaniecki, Z., Grudzień, K.: Determination of bulk solid concentration changes during granular flow in a model silo with ECT sensors. Chem. Eng. Sci. **64**(1), 20–30 (2009)

Ott, F., Herminghaus, S., Huang, K.: Radar for tracer particles. Rev. Sci. Instrum. **88**(5), 051801 (2017). https://doi.org/10.1063/1.4982942

Parker, D.: Positron emission particle tracking and its application to granular media. Rev. Sci. Instrum. **88**(5), 051803 (2017)

Ren, X.-H., Stapf, S., Blümich, B.: Magnetic resonance visualisation of flow and pore structure in packed beds with low aspect ratio. Chem. Eng. Technol. **28**(2), 219–225 (2005)

Schlageter, V., Besse, P.-A., Popovic, R., Kucera, P.: Tracking system with five degrees of freedom using a 2D-array of hall sensors and a permanent magnet. Sens. Actuator A-Phys. **92**(1–3), 37–42 (2001)

Schlageter, V., Drljaca, P., Popovic, R.S., Kučera, P.: A magnetic tracking system based on highly sensitive integrated hall sensors. JSME Int. J. Ser. C Mech. Syst. Mach. Elem. Manuf. **45**(4), 967–973 (2002)

Schröter, M., Lyv, C., Huang, J., Huang, K.: Challenges of 'imaging' particulate materials in three dimensions. Pap. Phys. **14**, 140015–140015 (2022)

Song, S., Li, B., Qiao, W., Hu, C., Ren, H., Yu, H., Zhang, Q., Meng, M.Q.-H., Xu, G.: 6-D magnetic localization and orientation method for an annular magnet based on a closed-form analytical model. IEEE Trans. Magn. **50**(9), 1–11 (2014)

Tao, X., Tu, X., Wu, H.: A new development in magnetic particle tracking technology and its application in a sheared dense granular flow. Rev. Sci. Instrum. **90**(6), 065116 (2019)

Vergne, C., Inácio, J., Quirin, T., Sargent, D., Madec, M., Pascal, J.: Tracking of a magnetically navigated millirobot with a magnetic field camera. IEEE Sens. J. 1 (2023). https://doi.org/10.1109/JSEN.2023.3264496

Wang, C., Lv, Z., Li, D.: Experimental study on gas-solids flows in a circulating fluidised bed using electrical capacitance tomography. Powder Technol. **185**(2), 144–151 (2008)

Wildenberg, S., Jia, X., Léopoldès, J., Tourin, A.: Ultrasonic tracking of a sinking ball in a vibrated dense granular suspension. Sci. Rep. **9**(1), 5460 (2019)

Windows-Yule, C., Seville, J., Ingram, A., Parker, D.: Positron emission particle tracking of granular flows. Annu. Rev. Chem. Biomol. Eng. **11**, 367–396 (2020)

Wong, Y.S.: Particle motion in relatively thin fluidised bed models. Chem. Eng. Sci. **61**(18), 6234–6238 (2006)